World Conference on Timber Engineering Oslo 2023

Performance Verification and Trial Design for High-rise Timber Frame Buildings with Buckling-Restrained Braces
Part.1 Connection and Frame Testing

Kazuki Tachibana[1], Hiroki Nakashima[2], Taisuke Nagashima[3], Ryota Minami[4], Toshio Maegawa[5], Nobuhiko Akiyama[6], Yoshihiro Yamazaki[7] and Takahiro Tsuchimoto[8]

ABSTRACT: A 10-story apartment building was designed with (1) multi-knife plate steel dowel connections for the joints, (2) BRBs as megastructural−columns for the seismic elements, and (3) GIR joints for the column bases. Tests were conducted to verify that these three types of high-strength connections performed as required. This paper describes the results of these tests and a discussion of the analysis method.

KEYWORDS: High-rise timber structure, Multiple Shear steel-to-timber joints, Buckling-restrained braces

1 INTRODUCTION

While demand for mid-rise and high-rise timber buildings has been increasing in recent years, non-timber structures are still dominate the market for mid-rise and high-rise buildings in Japan. One of the challenges in promoting the use of mid-rise and high-rise timber buildings is to ensure their seismic performance. In order to create a good role model, this study was designed to test a 10-story apartment building with mega-structural columns and Buckling-Restrained Braces (hereinafter referred to as "BRB"). [Fig. 1]

Part 1 describes the tests conducted for the trial design and their results. An analytical model is proposed and compared with test results to verify the validity of the analytical model.

2 CONNECTION TEST

2.1 INTRODUCTION

The Japanese standard [1] describe how to calculate the allowable shear capacity of steel dowel joints with steel inserted plate and with steel side plates, but they do not describe the case where multiple steel plates are inserted or the scope of application, for example, whether it is possible to use large-section glued laminated wood or large diameter drift pins. Here, shear tests were conducted to verify whether the shear strength could be obtained by a simple calculation. Specifically, as shown in Fig. 2, we verified whether the ratio of the number of steel dowels and the addition on the burden area (dowel length) were valid.

2.2 MATERIALS AND SPECIMEN

Fig. 3 shows an overview of the specimens: the A1 has 27 steel dowels inserted; the B1 and B3 have 5 steel dowels inserted; the A1 and B1 have 1 steel plates inserted; the

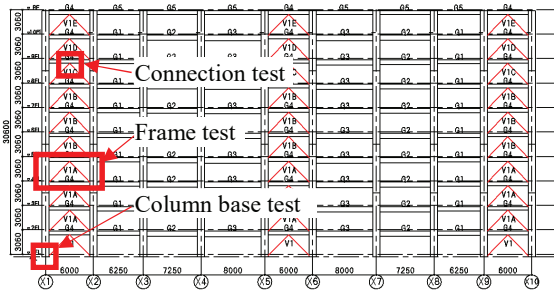

Fig. 1 10-story timber apartment (trial design)

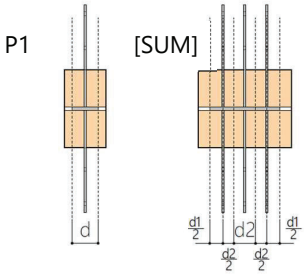

$$[\text{sum}] = \frac{d1}{d}P_1 + \frac{d2}{d}P_1 + \frac{d2}{d}P_1 \qquad \textit{Eq. 1}$$

Fig. 2 Length of steel dowel to bear the load

[1] Kazuki Tachibana, M. Eng., Sumitomo Forestry, Japan, tachibana_ kazuki @sfc.co.jp
[2] Hiroki Nakashima, M. Eng., Sumitomo Forestry, Japan, nakashima_ hiroki @sfc.co.jp
[3] Taisuke Nagashima, Ph. D Eng., Chief Researcher, Sumitomo Forestry, Japan, tsk-naga@sfc.co.jp
[4] Ryota Minami, M. Eng., Kumagai Gumi, Japan, ryota.minami@ku.kumagaigumi.co.jp
[5] Toshio Maegawa, Chief Researcher, Kumagai Gumi, Japan, tmaegawa@ku.kumagaigumi.co.jp
[6] Nobuhiko Akiyama, Dr. Agr., Senior Researcher, Building Dept., NILIM, MLIT, Japan akiyama-n92rg@mlit.go.jp
[7] Yoshihiro Yamazaki, Dr. Eng., Senior Research Engineer, Building Research Institute, Japan, y_ymzk@kenken.go.jp
[8] Takahiro Tsuchimoto, Dr. Agr., Chief Research Engineer, Building Research Institute, Japan, tutti@kenken.go.jp

https://doi.org/10.52202/069179-0201

B3 has 3 steel plates inserted. The timber was laminated Japanese larch E95-F270 with secondary gluing in the width direction, the steel plate was SS400 with a thickness of 12mm, and the steel dowels were SNR490B with a diameter of 20mm. The hole diameter for the steel dowel s was 20mm for the timber and 21mm for the steel plate. Steel dowels were 150mm long for A1 and B1, and 350mm long for B3, with tapered end. A slit of □-16 × 1,180 was cut out in the timber for steel plate insertion. The number of specimens was one for B1 and three each for A1 and B3

2.3 METHODS

Fig. 4 shows the testing machine performance and the test setup of specimen. The test specimen and jig were fixed by frictionally joining the left and right sides of the inserted steel plate. For displacement, the relative displacement of each steel plate to the timber was measured, and the average value was used as the deformation. The load was applied monotonically from the top of the column using a hydraulic jack while measuring the load, and was applied until the load dropped to 80% of the maximum load or until the joint was deformed more than 30 mm and lost its function as a joint.

2.4 RESULTS AND DISCUSSIONS

The experimental results are shown in Fig. 5. From the obtained displacements and loads, the yield capacity P_y and ultimate capacity P_u were obtained in accordance with "How to Obtain Yield Capacity and Ultimate Capacity Using Full Elastic-Plastic Model "[2].

2.4.1 NUMBER OF STEEL DOWELS

Fig. 6 compares the history curves of the A1 specimen with those of the B1 specimen, corrected for a steel dowel count ratio of 27/5 times. Fig. 6 shows that there is a proportional relationship between the number of steel dowels and shear strength.

2.4.2 NUMBER OF INSERTED STEEL PLATES

[Sum]B1 is the prediction of the B3 result from the B1 result based on Fig. 1. The [Sum]B1 and B3 results are compared in Fig. 7, which shows that [Sum]B1 is evaluated on the safe side with respect to B3.

Fig. 8 compares [Sum]A1 obtained from the A1 test result with the results of the B3 specimen multiplied by 27/5. This result also shows that [Sum]A1 is evaluated to be on the safe side compared to 27/5 of the B3 specimen.

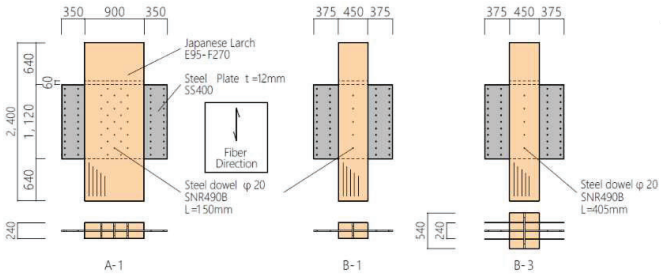

Fig. 3 Specimen detail

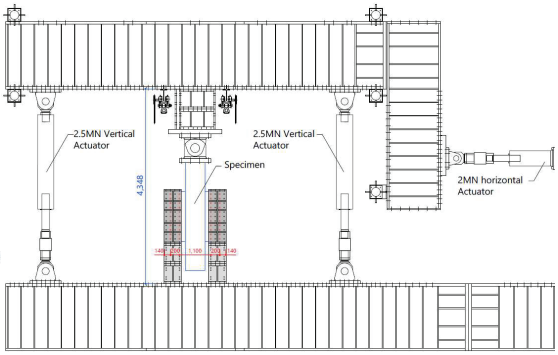

Fig. 4 Test setup of specimen

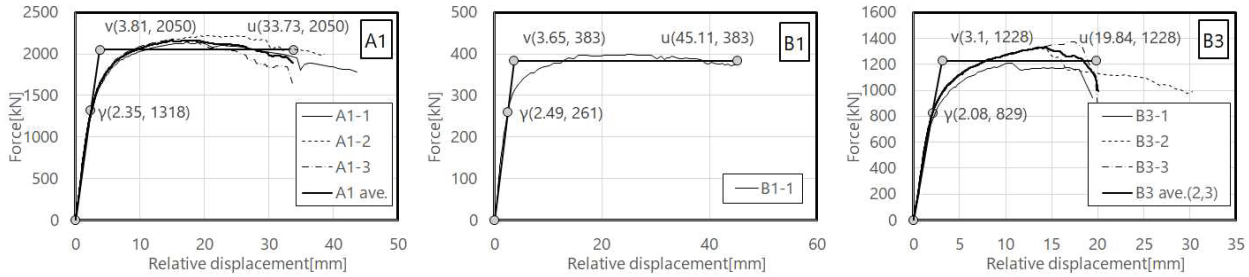

Fig. 5 Load-deformation relationships and Bi-liner carve

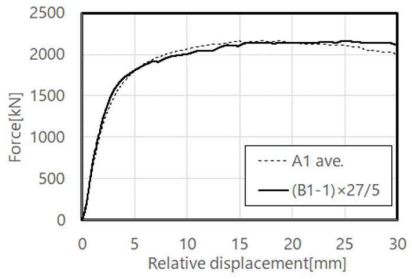

Fig. 6 Analyze impact of number of steel dowel

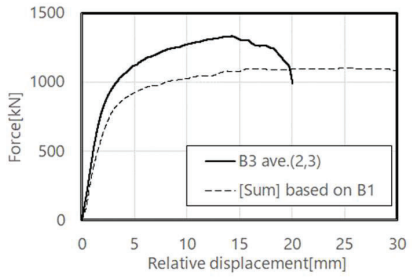

Fig. 7 Analyze impact of number of steel dowel

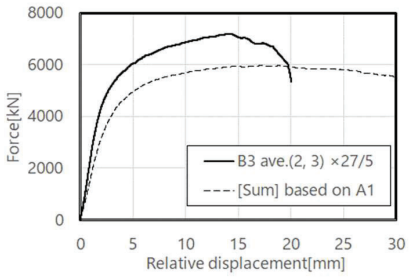

Fig. 8 Analyze impact of number of steel dowel

https://doi.org/10.52202/069179-0201

3 FRAME TEST

3.1 INTRODUCTION

Our trial design of a high-rise timber frame building has BRBs as the main seismic element. The design assumed that the BRBs yield first during deformation, and then the toughness of the BRBs is expected until the safety limit is reached. However, each joint of the frame is not a pin joint but a semi-rigid joint with rotational stiffness, and the frame bears a part of the seismic force after the BRB yields. The frame is designed so that the deformation of the frame is within the elastic range even at the safety limit, but it was confirmed experimentally that the load borne by the frame is as calculated and that the joints do not fail in bending under large deformation. (hereinafter referred to as "Frame test")

In order to estimate the axial force acting on the BRB joint during the frame test and to control the applied force, a cyclic test of the BRB alone (hereinafter referred to as "BRB test") was conducted in advance, and the load deformation of the BRB alone was confirmed up to the ultimate region.

3.2 BRB TEST

3.2.1 MATERIALS AND SPECIMEN

The BRB used for the test specimen was a BRB manufactured by Nippon steel engineering Co., Ltd. The specimen specifications are shown in Table. 1 and the design specifications are shown in Table. 2. Yield stress and strength are based on mill test report. The post-yield stiffness degradation rate was taken from the manufacturer's technical data [3]. The BRBs were custom-ordered with a yield capacity of 113kN and an ultimate capacity of 205kN, and end plates were added to the ends and bolted to the load jig and end plates.

3.2.2 METHODS

Fig. 9 shows the performance of the testing machine, the specimen setup, and the position of instrumentation. The polarity of the load and displacement was set to be positive on the tensile side. The loading method was cyclic loading with hydraulic jacks, which was repeated three times per a cycle. The loading schedule is shown in Table. 3, and the average value of the vertical displacement (7) and (8) of the jig column was considered to be equivalent to the displacement of the plasticized part and was used as the displacement for control.

Overall disp. $\delta_0 = (③ + ④ + ⑤ + ⑥) / 2$ ***Eq. 2***

Control disp. $\delta_1 = (⑦ + ⑧) / 2$ ***Eq. 3***

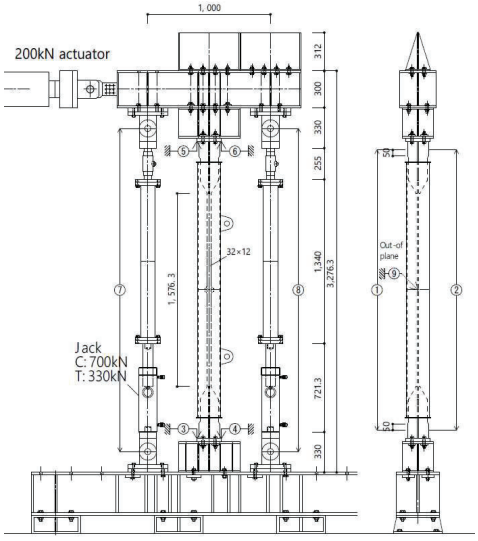

Fig. 9 Test setup of specimen

3.2.3 RESULTS AND DISCUSSIONS

Based on test result, the yield point and the 3%-L_p deformation point were read from the envelope curve and a bilinear (test) was created. The 3%-L_p deformation point was set at the maximum deformation at the first loading. The bilinear model obtained from the design values was designated as bilinear (design), and this graph was used in the analysis. These two bilinears are shown together in Fig. 10. The bilinear model based on theoretical values does not take into account the load rise, but we believe that this model is sufficient for the frame analysis, which is mainly

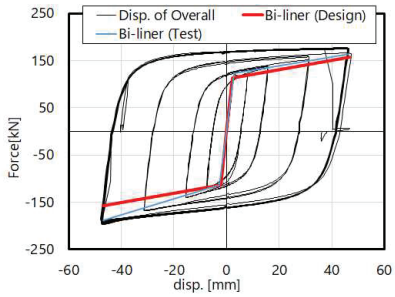

Fig. 10 Load-deformation relationships

Table. 1 Specimen specifications

Parts	Material	Size[mm]	Grade	Standard
Core	Steel plate	12×32	SN400B	JIS G 3136
Cover	Round steel pipe	φ191×4.5	STK400	JIS G 3444

Table. 2 Design specifications

Overall Length	L_0	2,476.3	mm
Yield (Core) Length	L_p	1,576.3	mm
Yield (Core) Area	A	384	mm^2
Young Modulus	E	205,000	N/mm^2
Elastic Stiffness	K_1	49.9	kN/mm
Stiffness reduction ratio	α	0.02	
Yield Stress	σ_y	294	N/mm^2
Strength	σ_u	534	N/mm^2
Yield strain	ε_y	0.00144	

Table. 3 Loading schedule

Target deformation			Cycle
0.5 δ_y	1.13	mm	3
δ_y	2.26	mm	3
L_p -0.5%	7.88	mm	3
L_p -1%	15.76	mm	3
L_p -2%	31.53	mm	3
L_p -3%	47.29	mm	1

https://doi.org/10.52202/069179-0201

Table. 4 The specifications of the members used for the frame specimen

Parts	Classification	Size[mm]	Grade	Standard
BRB (Core)	Rolled steels for building structure	12×32	SN400B	JIS G 3136
BRB (Core)	Carbon steel tubes for general structure	φ190.7×4.5	STK400	JIS G 3444
BRB (Joint)	Torshear type high strength bolt set	M16	S10T	JSS II-09
Beam	Structural glulam (Japanese Larch)	250×480	E95-F275	JAS
Column	Structural glulam (Japanese Larch)	375×720	E95-F275	JAS
Joint (side plate)	Rolled steels for general structure	t=12, 19	SS400	JIS G 3101
Joint (insert plate)	Rolled steels for general structure	t=12, 32	SS400	JIS G 3101
Steel dowel	Rolled steels for building structure	φ20	SNR490B	JIS G 3138

Table. 5 scale factor of the specimen

Length	Floor height	4/5
Section	Width	4/5
	Height	5/12
	Section(stress)	1/3

concerned with the first loading. The bilinear (test) model showed a difference from the bilinear (design) model in that the yield load was larger on the tensile side and the second-order slope was larger on the compressive side.

3.3 FRAME TEST

3.3.1 MATERIALS AND SPECIMEN

The BRB used in the frame tests were the same as those used in 3.2. The specifications of the members used for the frame specimen are shown in Table. 4 and the names of the parts are shown in Fig. 11. The ends of the BRBs were friction-bolted with high-strength bolts friction joints, accompanied by joint hardware and splice plates. Although frame tests were considered at full scale, the largest specimen was set up to match the testing laboratory's frame testing machine. The scale factor of the specimen scaled down from full-scale is shown in Table. 5. The specimen was also rotated 90°, so that the columns and beams were inverted as shown in Fig. 11. There are three types of connections between the beam-column hardware and the timber: C is the connection to the column, G is the connection to the beam, and B is the connection between the BRB and the beam. Joints C and G are drift pin joints with two steel plates inserted into the timber, and joint B is a bolted joint with steel plates on both sides of the timber. The reaction force fulcrums of the test specimens were made by extending the joint hardware steel plates and connecting them to a pin bearing and a roller bearing, respectively. Each joint must have sufficient bearing capacity and deformation capacity to allow the BRBs to withstand the ultimate load. The number of steel dowels was determined so that the short-term shear capacity of joints C, G, and B of the specimen would be sufficient for the axial force of the frame generated when the BRB restoring force was at its maximum, and the arrangement of the steel dowels was determined so that the rotational stiffness would be as small as possible. For joint B, a steel dowel joint with the steel-plate-insertion was planned, but since there was a possibility that the BRB would twist the beam due to the stress of the BRB during loading, bolt joint with the steel side plate was used in the hope that the torsional resistance

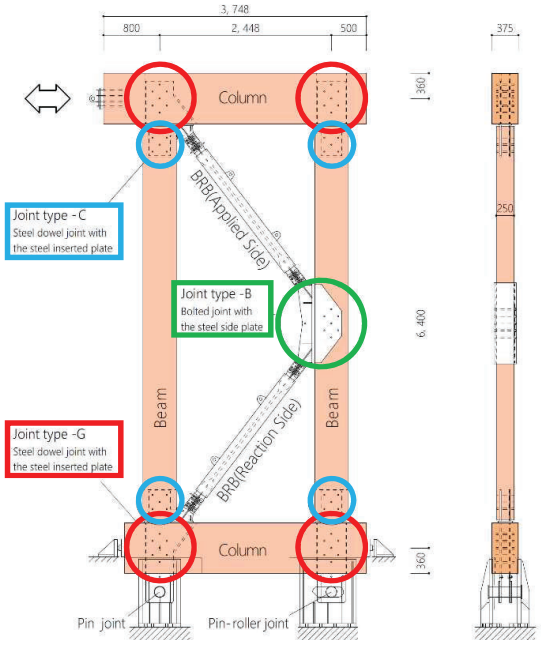

Fig. 11 Test setup of specimen

of the beam would be effectively transmitted. The short-term shear capacity of joint B is smaller than the maximum axial force of the frame and is 1.2 times the frame axial force at yield. The diameter of the holes drilled in the steel plate and timber for each joint was the same as in "2. CONNECTION TEST" for steel dowel joints with the steel-plate-insertion, and 22mm holes were drilled in both the plate and timber for the bolted joint for steel side plate, and φ20 bolts were used.

3.3.2 METHODS

The loading schedule for the tests is shown in Table. 6. Based on the results of the BRB stand-alone tests, the loading was controlled using the value of axial deformation δ_{b1} of the BRB up to the yield displacement δ_y of the BRB at the structure surface, and was repeated 3 times each at $\pm \delta_y \times 0.5$ and $\pm \delta_y$ in alternating cycles. The load was then repeated 3 times alternately at ±1/300, ±1/200, ±1/150, ±1/100, ±1/75, and ±1/50 of the deformation angle of the specimen, respectively, and after 1/50, the load was monotonically applied in the tensile direction until failure. The test was not conducted from 7C to 9C because the target interlaminar deformation angles of 7C to 9C were reached in the first cycle up to

https://doi.org/10.52202/069179-0201

6C. In the frame tests, applied loads, overall displacements, rotation angle and shear deformation of each joint element, and axial displacement of the BRB were measured. The horizontal displacement of the specimen δ was determined by the relative displacement of columns

3.3.3 RESULTS AND DISCUSSIONS

The load-deformation relationship and envelope are shown in Fig. 12. 1C to 6C, the deformations are significantly different on the positive and negative sides.

This is partly because the displacement was controlled by the axial displacement of the BRB, but the main reasons for this are the clearance of the bolted joints in the Joint B hardware and the one-sided effect of the hardware, which resulted in a large slip on the tensile side. In each of the subsequent cycles, the load on the compression side was slightly higher than that on the tension side.

Table. 6 Loading schedule

	Target	
	BRB disp. [mm]	Angle of deformation [rad]
1C ～ 3C	1.13	-
4C ～ 6C	2.26	-
(7C ～ 9C)	-	1/300
10C ～ 12C	-	1/200
13C ～ 15C	-	1/150
16C ～ 18C	-	1/100
19C ～ 21C	-	1/75
22C ～ 24C	-	1/50
25C	-	Pull

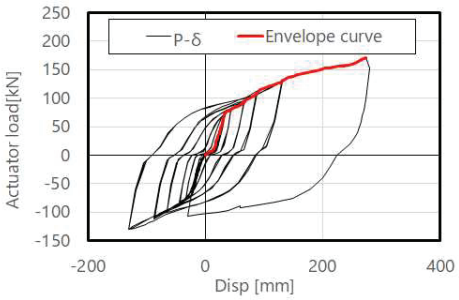

Fig. 12 Test result (P-d carve)

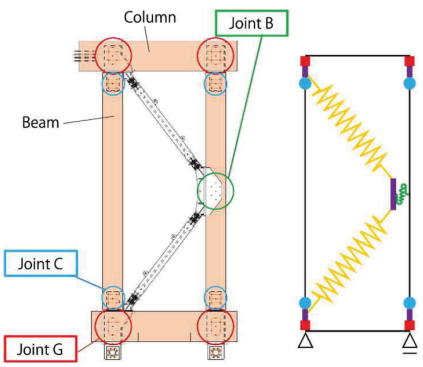

Fig. 13 Analysis model

3.4 ANALYSIS MODEL

3.4.1 JOINT

An overview of the modeling is shown in Fig. 13. The timber is modeled as a beam element, and each joint and BRB are modeled with the nonlinear springs shown in Fig. 14. The beam elements (▬) between joint C (■) and joint G (●), between BRB and joint B (), were input as rigid bodies. Joint C (■) was modeled with rotational and shear springs, and joint G (●) with rotational and axial springs. For joint B, only the shear spring acting in the vertical direction was input, assuming no rotation. The stiffness and bearing capacity of the joints were determined by the European Yield Theory [1, 4] for performance per a steel dowel and corrected by the burden area based on the results obtained in 2. After confirming that the mode of failure did not change with the difference in burden area, these results were added together.

3.4.2 BRB

The BRB was assumed to be a nonlinear spring of an axial spring. For the modeling of BRBs evaluated as axial springs, BRBs were synthesized from the stiffness of the centrally buckling-constrained core section and the stiffness of the cross section at the ends. If the stiffness of the core section is k_{B1} and the stiffness of the end cross section is k_{B2}, the composite stiffness $k_{BRB}=1/(1/k_{B1}+1/k_{B2})$. From the cross-section of the plasticized section of 12mm x 32mm and the yield point strength of 294 MPa, the yield capacity is 113kN and the axial stiffness k_{B1} is 49.9kN/mm. The stiffness k_{B2} of the cross section was determined to be 300kN/mm for the axial stiffness except for the plasticized section. The ultimate strength of the plasticized section is 400 MPa and the stiffness reduction ratio $\alpha = 0.02$, and the stiffness is obtained by synthesizing the secondary slope in the same manner, assuming that the ends do not yield. The obtained bilinear curve of BRB is shown in Fig. 15.

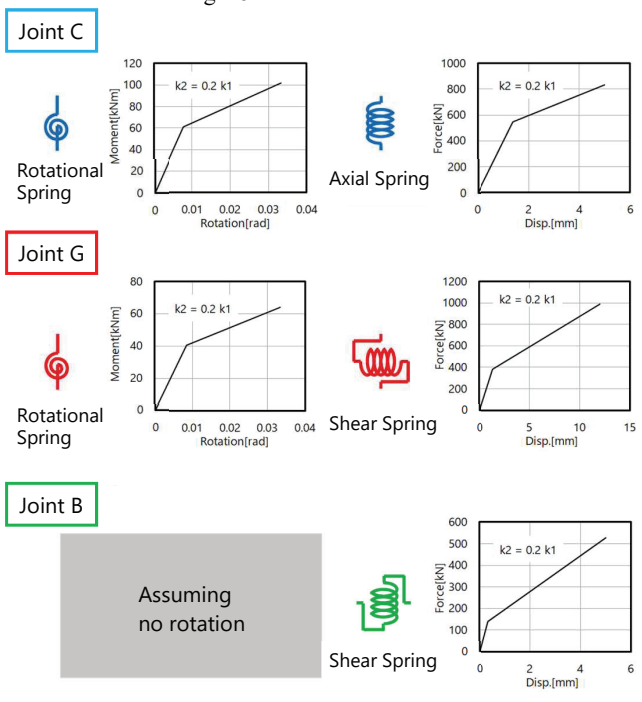

Fig. 14 Analysis model (each joint)

https://doi.org/10.52202/069179-0201

3.4.3 ANALYSIS RESULTS

For the orange graph in Fig. 16, the solid line shows the test results and the dotted line shows the analytical model applied up to 1/20 rad by pushover analysis. The solid line is a graph of the load P and displacement δ extracted at the first deformation experienced in the positive (tensile) direction from the start of the test and when the load value is greater than or equal to the load value recorded previously. The timing of the yielding of the joints during the analysis is noted in the figure. The shear and axial springs were elastic, and the rotational springs yielded at joints G and B, in that order. At these two timings, the four joints yielded almost at the same time. A comparison of the experimental and analytical jack load-deformation relationships for each joint is shown in Fig. 17.

(A) Joint C - Rotation angle

At all locations below 125kN where failure occurs, the analytical and experimental results agree well. The calculated yield rotation angle was 1/130 rad, and yield deformation was not reached.

(B) Joint G - rotation angle

Experimental and analytical values are in good agreement up to a cycle of 100kN and 1/75 rad of the specimen in terms of load value; above 100kN, the experimental value exceeds the analytical value in the large deformation region.

(C) Joint C - horizontal shear deformation

For the applied force side (U), the rotational component was subtracted from the displacement measured on the underside of the timber to obtain a value, so there is some variation in the trajectory of the graph, but the displacement is within about 1mm, which is the clearance of the joint. In North-D_C-S_H, the joint hardware is directly connected to the pin joint but there is some movement, and there is slip until the column member resists. (There are restraints at both ends of the below column to prevent horizontal movement.)

(D) Joint G Load - Vertical shear deformation

Slip of 1mm or less is observed at load 0 in general, which may be due to the effect of the gap around the steel dowel. In the analysis, the joint did not yield up to about 170kN, but in the experiment, plastic deformation occurred around 150kN on the South side at 1/50 rad or later when the joint was pulled apart; when the displacement of South- D_G-S reached 4.4mm, the joint cracked and the displacement increased to 8.8mm at once.

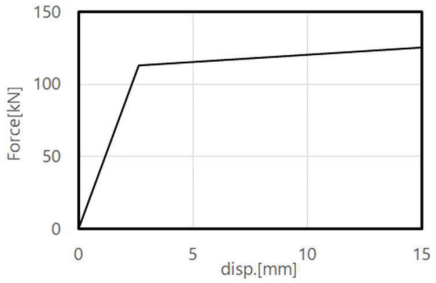

Fig. 15 P-d carve (BRB, bi-liner)

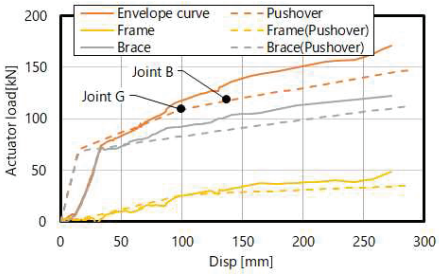

Fig. 16 P-d carve (Envelop curve and Analysis)

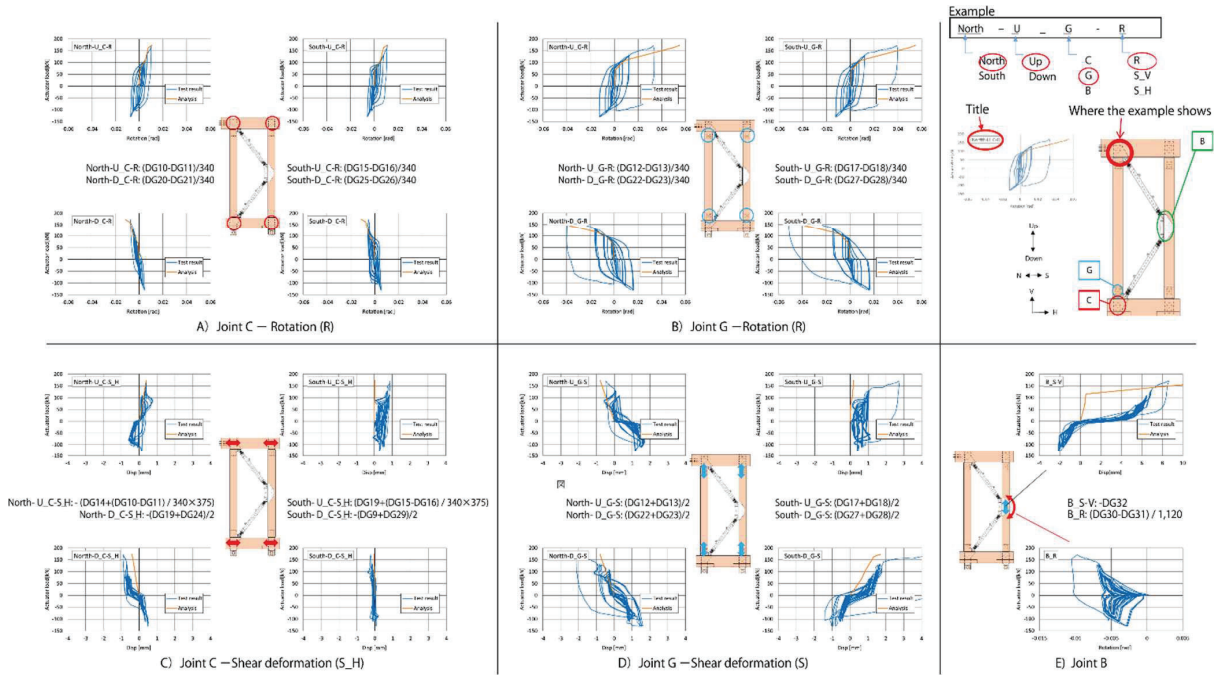

Fig. 17 Comparison of experimental and analytical results (each joint)

https://doi.org/10.52202/069179-0201

Table. 7 The specifications of the members used for the column-base joint specimen

Parts	Classification	Size[mm]	Grade	Standard
Column	Structural glulam (Japanese Larch)	300×900	E105-F300	JAS
GIR	Deformed steel bar (threaded section rebar)	D29	SD345	JIS G 3112
Steel shoe	Rolled steels for building structure	t=16, 22, 32	SN400B	JIS G 3136
Glue	Epoxy	—	—	—

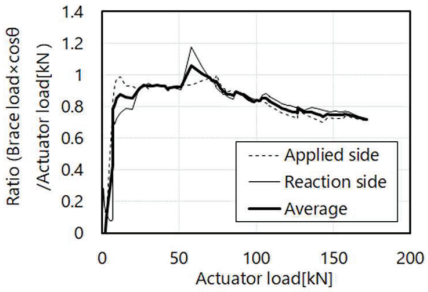

Fig. 19 Ratio of force borne by the brace

E) Joint B

In the experiment, the joint slipped about 4mm in the vertical direction. This is thought to be due to the effect of the gap of the hole on the diameter of the joint B joint. This is also evident in the initial slip of the overall deformation. The reason for the rotation of joint B is thought to be that the deformation of the frame created a hinge in the cruciform steel portion of the brace end, and because of the distance between the attachment points of the connection hardware B, the expansion and contraction of the brace created an angle in the connection hardware.

3.4.4 ESTIMATION OF HORIZONTAL LOADS TO BE BORNED BY THE BRB

In creating the orange lines in Fig. 16, the deformations δ_{b1} and δ_{b2} of the two BRBs were recorded at the same time. The axial force of the brace is estimated from these deformations and the envelope in Fig. 10, BRB test result. The load borne by the BRB during the frame test can be assumed to be the horizontal component of the estimated axial force of the BRB. (Horizontal load borne by BRB = BRB estimated axial force × cosθ [where cosθ = 2,448mm / 4,028mm]). The load-bearing ratio is the ratio of the BRB load divided by the actuator load P. The obtained load-bearing ratio of the BRB is shown in Fig. 19. Initially, the value is small due to slip, but it soon approaches 1.0 and remains at about 1.0 when a force of about 10kN is applied, and after P reaches the yield capacity, the burden ratio decreases to about 0.8. This result indicates that the forces acting on the upper and lower BRBs were almost the same. As a result, there was almost no bending moment of the beams due to the disproportionate force of the braces.

Grey line in Fig. 16 shows the average of the loads on the upper and lower BRBs and yellow line in Fig. 16 shows the load on the frame (the envelope curve of the solid orange line in Fig. 16 minus the load applied to the BRB [Grey line]). From these results, it can be confirmed that up to the yield load, the brace alone resists the load. After the yield load, the frame bears about 20% of the load, but no damage was observed up to 1/50 rad, confirming the integrity of the frame.

4 COLUMN-BASE JOINT

4.1 INTRODUCTION

As buildings rise in height, axial forces (e.g. dead weight) acting on columns increase, and it is known that axial forces affect the moment capacity of column base. Therefore, in order to model the first-floor column bases of a 10-story timber-frame apartment building and to create an *M-N* interaction curve showing this effect, bending tests were conducted using the column axial force as a parameter while applying a vertical load. The test results were used to validate the modeling and the method used to model the first-floor column bases.

4.2 MATERIALS AND SPECIMEN

Fig. 18 shows an overview of the test specimen. Table. 7 shows the specimen specs. The lumber used was E105 F300 laminated larch of symmetrical mixed-grade. The steel shoe was made of SN400B and SN400C, which were used to connect the timber to the slab. The first-floor columns were assumed to be 900mm x 900mm in cross section, but the cross section of the specimen was 300mm × 900mm with the cross section multiplied by 1/3 in the depth direction due to the capacity of the jacks to apply vertical loads and horizontal forces. A maximum axial force of 5,400kN is considered to act on the assumed first-floor columns in the design. The axial force parameters were 1,800kN (test symbol N1800), which is 1/3 of the assumed load, 900kN (test symbol N0900), which is 1/6 of the assumed load, and no axial force (test symbol N0000), and one of each was tested. The specimen setup is shown in Fig. 20 and Fig. 21. The height of the force point was set to 2,500mm, the height of point of contraflexure obtained from the analysis. The height of N0900 and N1800 timber was set to 1,925mm, subtracting

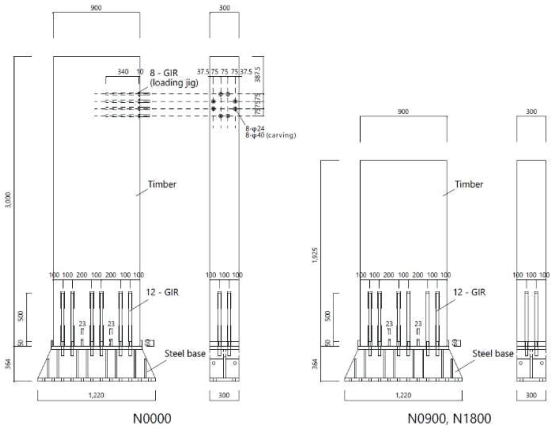

Fig. 18 Specimen detail

https://doi.org/10.52202/069179-0201

the height of the jig. The height of the N0000 timber was assumed to be 3,000mm, including the extra length. The steel shoe was also multiplied by 1/3 in the depth direction. For shear forces acting on the timber column ends, SN400B steel plates, 22mm thick and 50mm high, welded to the top of the steel shoe was designed to act as shear keys and bear the shear forces. Four shear keys were placed at the locations that divide the timber into three equal parts in the width direction and at both ends. Shear keys were inserted into grooves 23mm wide and 60mm deep on the timber side. The Glued in rods (hereinafter referred to as "GIR") for column bases were machined from SD345 D29. The gluing section was 500mm long, with a plasticized section 22mm in diameter and 50mm long, and an M27 screw machined into the end. The GIR used can be considered to have three possible failure modes: (1) failure of the plasticized section, (2) failure of the adhesive section, and (3) collective shear failure of the timber section. The upper limit of the maximum bearing capacity of the plasticized section was assumed to be lower than the lower limit of the maximum bearing capacity of the adhesive section, and it was judged that (2) would not occur. In addition, for the collective shear failure of timber, since the perimeter area surrounded by four GIRs is larger than the perimeter area of one GIR × 4 GIRs, it was judged that (3) collective shear failure of timber would not occur.

From the above, it was confirmed by manual calculations that the joints of GIR fail prior to the plasticized part during pull-out. To control the strength of the plasticized section, an upper strength limit of 550N/mm^2 (=210kN) was ordered, and the actual value (mill test report) was 554 N/mm^2 The JIS standard values and mill test report values are shown in Table. 8. Epoxy resin adhesive (Home Connector Co., Ltd.: AHC-E) was used as the adhesive. After the adhesive had cured, the threaded portion of the GIR was fixed with a double nut while measuring the strain gage value so that the initial tension of the GIR was approximately 10kN. For the specimens with axial force, the nuts were fastened after the axial force was applied.

4.3 METHOD

The specimen with axial force was loaded vertically by vertical jacks at both ends through a pin jig at the top. The pin jig was in contact with the upper timber face and the sides were clamped by brackets with a clamping mechanism. The tightening mechanism was adjusted at the maximum deformation of each cycle because a gap was created on the sides due to the pin fixture when a horizontal force was applied. The distance from the top of the steel frame trestle to the center of the pin was assumed to be 2,500mm at the height of point of contraflexure. For the specimen without axial force, a 3,000mm-high timber was used and eight GIRs were joined so that the force point was at 2,500mm. In this test, deformation was controlled by the angle of rotation between the timber and the steel shoes. The axial force of the GIRs was calculated from the average of the axial strains of the two GIRs. Two strain gauges were placed at the axisymmetric position of the plasticized GIR for the purpose of measuring the axial force of each GIR.

The loading schedule was as follows: three cycles of positive/negative alternating loading at angles of rotation θ of 1/900, 1/450, 1/300, 1/200, 1/150, 1/100, 1/75, and 1/50 rad for the column bases between timber and steel shoes; 1/30 rad of positive/negative alternating loading; and then monotonous loading until failure. For N0000 and N1800, the deformation was controlled by the rotation angle θ. For N0900, it was determined that the rotation angle θ could not be used to control the deformation due to cracking and separation of the timber observed in the N1800 test. The corrected rotation angle θ' used for control is shown in Eq. 4. The corrected rotation angle θ' was corrected using the displacement $\delta_{1/100}$ at 1/100 rad, assuming that the horizontal displacement δ is proportional to the actual rotation angle.

$$\theta = \begin{cases} \theta & (\theta < 1/100\,rad) \\ 0.01 \cdot \delta/\delta_{1/100} & (\theta \geq 1/100\,rad) \end{cases} \qquad \textit{Eq. 4}$$

4.4 RESULT

Fig. 22 through Fig. 24 show the M-θ relationships obtained from the tests. The GIR plasticized section yielded first at the moments shown in each figure, and the bearing capacity decreased with rupture. However, in the case of N0000 and N0900, cracking occurred near the joints before the GIR plasticized section ruptured, and in the case of N0900 and N1800, cracking and separation of

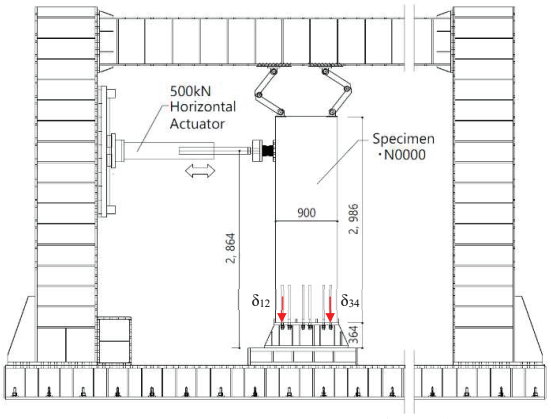

Fig. 20 Test setup of specimen (N0000)

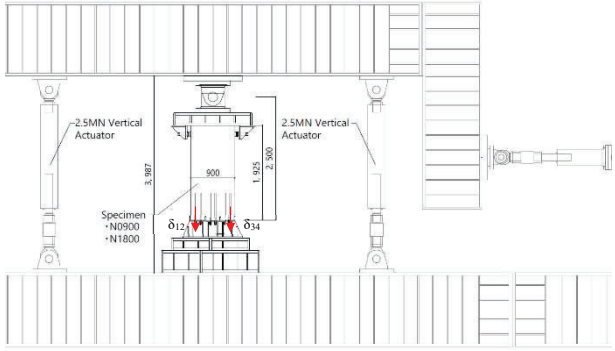

Fig. 21 Test setup of specimen (N0900, N1800)

Table. 8 the value of standard and mill test report

	σ_y N/mm^2	σ_u N/mm^2	YR %	Elongation %
Standard	345~440	Over 490	Over 80	Over 19
Report value	392	554	71	23

https://doi.org/10.52202/069179-0201

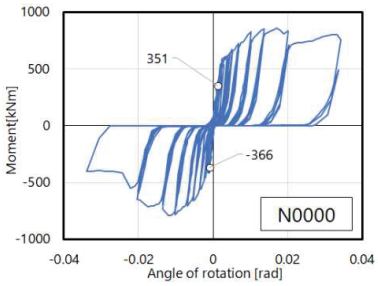

Fig. 22 Moment-rotation relationships(N0000)

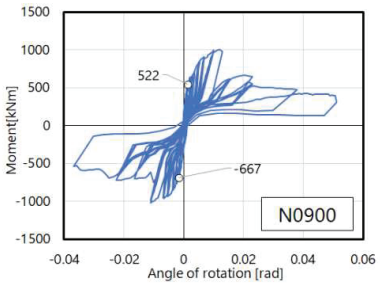

Fig. 23 Moment-rotation relationships(N0900)

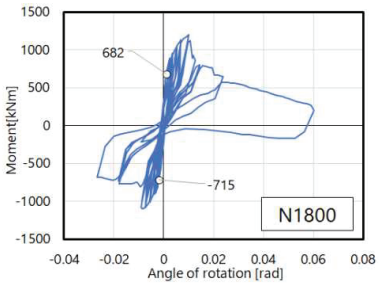

Fig. 24 Moment-rotation relationships(N1800)

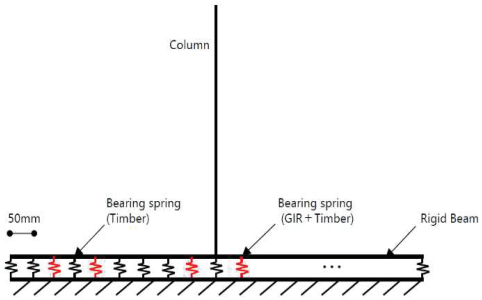

Fig. 25 Multi-spring model

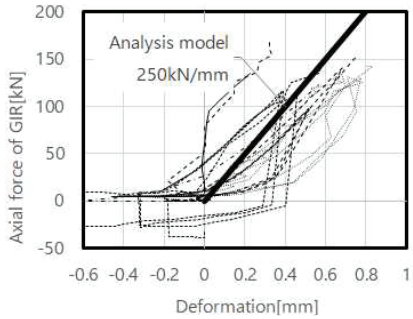

Fig. 26 P- δ curve (GIR)

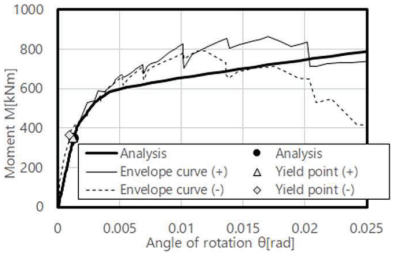

Fig. 27 Moment-rotation relationships(N0000)

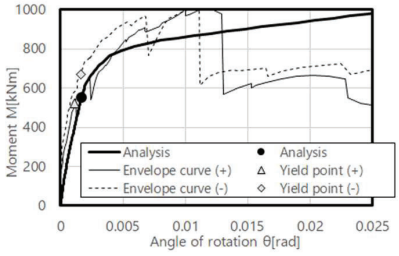

Fig. 28 Moment-rotation relationships(N0900)

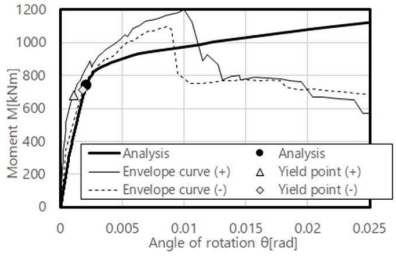

Fig. 29 Moment-rotation relationships(N1800)

the timber occurred as described above. Based on the above, the performance of this column-base joint was allowed up to the yield of the GIR plasticized section.

4.5 ANALYSIS MODELS

4.5.1 MULTI SPRING MODEL

The specimen was modeled with a multi-spring model using beam elements shown in Fig. 25. The analytical model consisted of rigid beams placed parallel to the ground plane and timber beam elements with a cross section of 300 x 900. The rigid beams were split at 50mm pitch, and GIR springs were placed at the same locations as the specimen. The ground plane was input with a surface pressure stiffness spring with stiffness acting only in compression.

4.5.2 EMBEDMENT STIFFNESS

For the embedment stiffness of the multi-spring model, k_{0c}=25N/mm^3[5] was used. For both ends of the rigid beams, 187.5kN/mm was used because the burden area is 1/2 that of other contact points. For yield capacity, a reference bearing capacity of 25.4MPa [1] was used.

4.5.3 GLUED IN RODS

The relationship between axial force and lifting (δ_{12}, δ_{34}) of GIRs obtained from all test results is shown in Fig. 26. The lifting displacement was the average of the vertical relative displacements of the front and back of the timber. From these results, the GIR stiffness k_{GIR} was read as 250 kN/mm, indicated by the thick red line in the figure, and used in this study. k_{GIR} is the composite stiffness obtained by connecting the stiffness k_f of the GIR anchorage section and the stiffness k_y of the plasticized section in series. k_f is obtained as 298kN/mm from k_y = 1,158kN/mm. Based on these results, a value of 500kN/mm was entered for the two GIR springs in the analytical model. α = 0.0088 was used for the GIR stiffness reduction rate, assuming that the elongation reaches the tensile strength at 12%.

4.6 DISCUSSIONS

4.6.1 COMPARISON OF ANARITICAL AND TEST RESULTS

To validate the analytical model proposed in 4.5, the moment-rotation angle relationship of the test results and the analytical results were compared in Fig. 27 through Fig. 29. The analytical results tended to be closer to the less stiff envelope of each positive and negative envelope of the test results. For the analysis results shown in Fig.

https://doi.org/10.52202/069179-0201

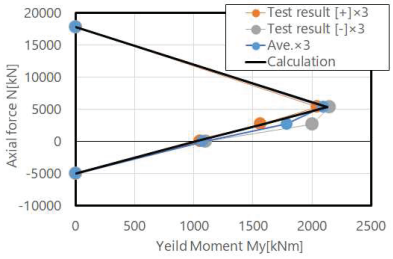

Fig. 30 M-N interaction curve (Section: 300×900)

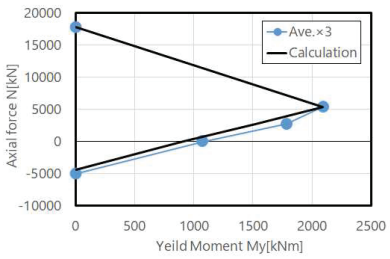

Fig. 31 M-N interaction curve (Section: 900× 900)

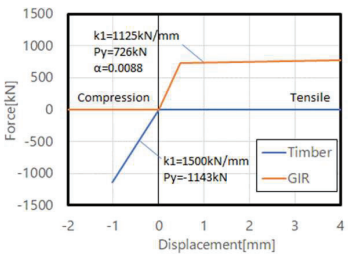

Fig. 32 Springs used for analysis

27 to Fig. 29, the yield point of GIR was taken from the mill test report value (f_y=392 MPa). The *M-N* interaction curve was prepared from the yield moment obtained and is shown in Fig. 30. It was confirmed that the analytical and experimental values were generally consistent.

4.6.2 M-N INTERACTION CURVE FOR ANALYSIS, AND VERIFICATION

The first-floor column cross section of the building under study is 900mm x 900mm. The column cross section is square. This means that in the width direction, the columns have the same configuration as the 300mm x 900mm columns used in the experiment (GIR and shear key locations), and the column cross section on the first floor is the same as three 300mm x 900mm columns in the depth direction. Here, the tripled test results are compared with the results of the analysis on the 900mm x 900mm cross section. In Fig. 31, the test results multiplied by 3 are compared with the analytical results (design specifications) using the lower limit of the reference value for yield strength of deformed bars (f_y = 345 MPa). Fig. 32 shows the parameters of each spring used as analysis conditions. It was confirmed that the values of the design specifications obtained from the reference values were inside the experimental values, i.e., on the safe side. The test ratio of the base metal at *N*=5,400kN was 0.97. The validity of the break point position was confirmed because the failure mode would change if the axial force increased beyond this point.

5 CONCLUSIONS

Multi knife-plates steel dowel connections

1. If the distance between dowels is sufficient, shear performance is proportional to the number of dowels.
2. As a simple calculation method, Multi knife-plates steel dowel connection was confirmed that the addition rule based on the burden area can evaluate.

Frame-testing

1. Using the simplified calculation method obtained in Section 2, the experimental results could be simulated with accuracy.
2. We checked the stress sharing ratio between the brace and the frame, and confirmed that almost no bending moment is applied to the beam ends until the brace yields.
3. Slip of about 4mm was observed at the connection covered by the steel plate. This was due to the clearance of the specimen. (2mm timber + 2mm steel plate) This slip deformation may have contributed to the slip in load de formation relationship.

Column-base joint

1. The performance of the column-base joints with GIR was verified through experiments to develop an *M-N* interaction curve that evaluated the effect of axial forces.
2. It was found that a multi-spring model using embedment stiffness k_{0c}=25N/mm^3 and the lower limit of the reference value for the yield strength of deformed steel bars could be used to model joint performance considering the effect of axial forces.

ACKNOWLEDGEMENT

This research was conducted as part of "Innovative technology for maintenance and management of construction and infrastructure and for disaster prevention and mitigation" in Public/Private R&D Investment Strategic Expansion PrograM (PRISM) add-on item "R&D Project for tall wood building for saving construction site of recovery housing "under the leadership of Japanese Cabinet Office.

REFERENCES

[1] Architectural Institute of Japan: Standards for Structural Design of Timber Structures, 2006.12F
[2] Japan Housing and Wood Technology Center, Allowable Stress Design of Wooden Houses with Post and Beam Construction System (2017 ed.)., 2017.3, p. 301
[3] Nippon steel engineering Co., Ltd., Unbonded Technical Data Design Edition, p3-3, 2019.4.
[4] Johansen K W: Theory of Timber Connections, International Association of Bridge and Structural Engineering, Publication No. 9, Bern, Switzerland, pp. 249-262, 1949.9
[5] Nagashima, T., Tachibana, K., Yano, M. and Ohashi, Y.: Design methods for post-tensioned timber shear walls (Part 1). Triangular embedment stiffness and behavior in the elastic range, Journal of Structural and Construction Engineering, Vol. 85, No.770, pp. 539-549, 2020.4

NOTE

・Regarding to 2, 3.3, 4, these tests were conducted at the Central Testing Laboratory of the Japan Testing Center for Construction Materials.
・Regarding to 3.4, this test was conducted at the Structural Laboratory of Sumitomo Forestry Tsukuba Research Institute.
・Midas iGen Ver.900 was used for the analysis study.